Modelling Local Seismograms of French Nuclear Tests In Taourirt Tan Afella Massif, Hoggar, Algeria

Stéphane Gaffet, B. Massinon, J.-L. Plantet, Y. Cansi

Geophys. J. Int. (1994) **119**, 964–974

Modelling local seismograms of French nuclear tests in Taourirt tan Afella massif, Hoggar, Algeria

S. Gaffet,[1] B. Massinon,[2] J.-L. Plantet[2] and Y. Cansi[2]

[1] *Institut de Géodynamique, 250 rue Albert Einstein, Sophia-Antipolis 1, 06560 Valbonne, France*
[2] *Laboratoire de Détection et de Géophysique, BP 12, 91680 Bruyères-le Châtel, France*

Accepted 1994 June 10. Received 1994 June 10; in original form 1993 October 18

SUMMARY

The influence of topography on the shape and amplitude of seismograms recorded at short distances is investigated for a set of nuclear explosions detonated in the Taourirt tan Afella mountain, Hoggar, Algeria, which was the French nuclear test site during the 1960s. The wavefield observed on one side of the mountain compared to that on the other shows a large-amplitude phase generated by reflection of the direct field inside the mountain. This phase is back-diffracted and can be seen in one azimuth and not in the opposite. The existence of such a phase depends on the source location inside the mountain. The amplitudes of standard phases are also modified with a factor of 2.5 by the topography between observations made in one azimuth compared to the others.

Key words: nuclear explosion, numerical modelling, site effect.

1 INTRODUCTION

The French nuclear test site used in the 1960s is located in the Hoggar massif (Fig. 1), 4 km west from In Eker, and 150 km north from Tamanrasset in the south of Algeria. The topography has been processed with GMT software (Wessel & Smith 1991). The test site is located in a granitic massif, the Taourirt tan Afella (5°2′ N; 24°3′ N), which is intruded in two gneiss series (Fauré 1972; Boullier & Bertrand 1981). The massif is intruded to the west side of a 1 km thick mylonitic zone (Fig. 2, from Fauré 1972). This zone, approximately oriented N–S separates the In Eker gneiss series (west side) and the Tefedest gneiss series (east side). Both series present a N–S schistosity. The area around the massif is covered by a thin layer of sand. The massif is 8 km long in the N–S direction and 5.6 km wide in the E–W direction and has a maximum height of 2000 m in a region with 1000 m mean elevation.

The study is an analysis of the relation between topography and waveform of the French explosions detonated in the Taourirt tan Afella massif. This study concerns the influence of the topography on the ground motions at local distances (i.e. from 1 km to 30 km) with the aim of understanding the waveforms observed in the N–S and E–W azimuths at BRI (approximately 2 km south-west from the explosions studied), BRIII (15 km west), INA (i.e. In Amguel, 30 km south). Teleseismic propagation is not accounted for here.

2 DATA COLLECTED

Thirteen underground explosions were detonated in the massif between November 1961 and February 1966 (see Table 2). Three sets of the recorded ground velocities are displayed in Fig. 3, which correspond to the explosions Jade, Opale and Rubis respectively. Only Rubis has been recorded at short distance (1.73 km) from the source at BRI. All explosions have been recorded at distances of around 15 km at BRIII and 30 km at INA.

The shape of the ground-velocity waveform differs greatly between these three explosions. The recordings at BRIII and INA for Rubis show pure *P* wave and Rayleigh wave. The recording of Opale at INA shows a longer surface wave train on the horizontal component. The greatest difference is found for recordings of explosion Jade which shows a long and strong coda associated with surface waves at BRIII and INA. These differences may be explained by different causes, i.e. explosion working (spalling, coupling), water saturation in the source region (and its evolution between each experiment), or surrounding geological structures and topography which induce multipathing and amplification effects.

3 STUDY

Teleseismic influence of the tan Afella topography shape has been detailed by Rocard (1964) and McLaughlin & Jih

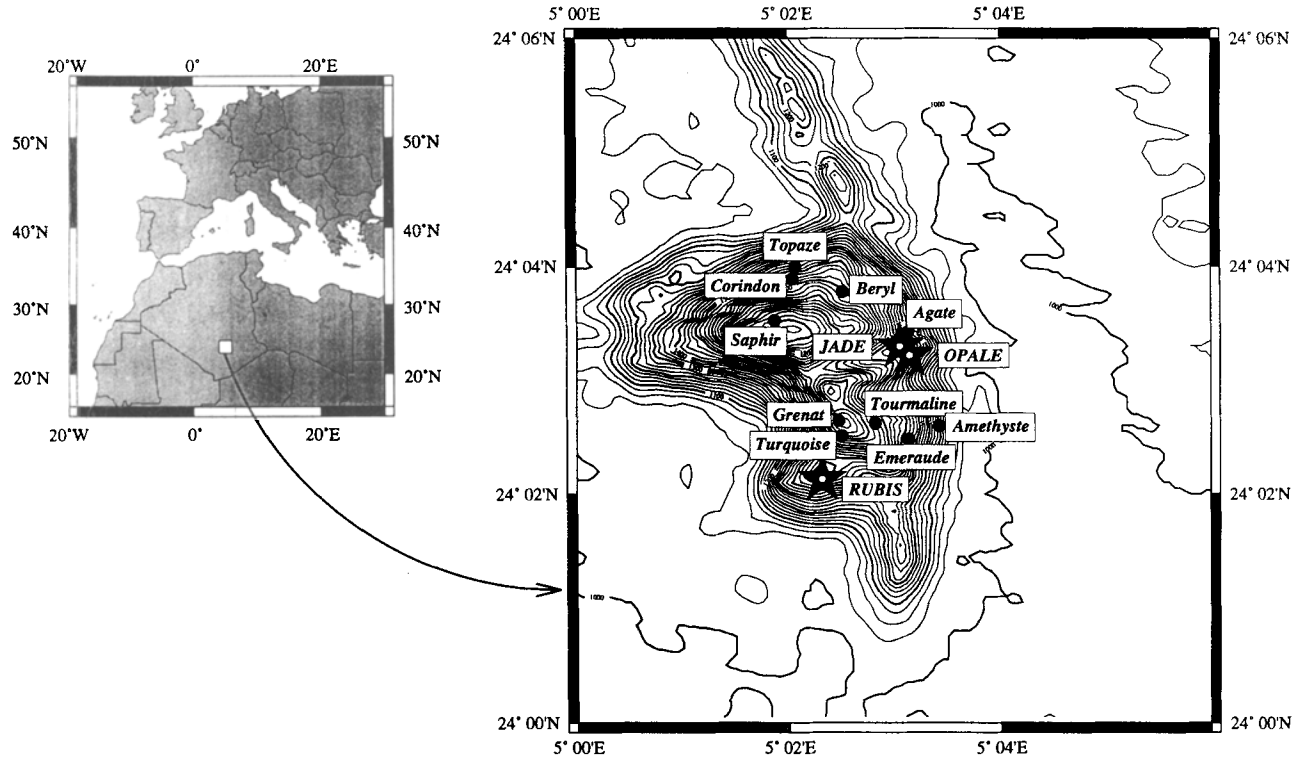

Figure 1. Location of 1960s French nuclear test site. Explosions are depicted with black circles and stars. Stars are used for Jade, Opale and Rubis, the explosions examined in this study.

(1988). Our main objective here is to understand the ground displacement waveforms at local distances (less than 30 km) in both N–S and E–W azimuths, in relation to the location of the shot inside the massif and to the azimuth of recording. To realize this objective, the global response of the Taourirt tan Afella structure (Duclaux & Michaud 1970; Munier 1982) is considered to be made up of both topography and crustal structure responses. The total displacement field generated by topography and crustal structure is made of multiple diffractions between topography and crustal structure. This implies that it is impossible to linearly separate the topographic effect from the underground-structure effect. The site effects presented below are related to the topography alone without taking into account the underground structure below it.

The results presented below are relative to the topographical effects of Taourirt tan Afella. They show the ground displacement modifications induced by (i) the topography shape and (ii) the detonation location inside the mountain. The numerical method used for computation is the discrete wavenumber–boundary integral equation method (Bouchon & Aki 1977; Gaffet & Bouchon 1989). The wave-propagation velocities are $\alpha = 6\,\mathrm{km\,s^{1}}$ and $\beta = \alpha/\sqrt{3}$, and the source–time function is a Ricker pulse.

Figure 4 shows, as reference, the ground velocities obtained for an explosion buried at 300 m depth under a flat surface. The only waves generated are the direct P wave followed by the Rayleigh wave of lower amplitude.

Preliminarily, an observational analysis is made with two fictitious explosions located in both sides of the massif along a NW–SE section as shown Fig. 5. The explosions are buried at 290 m and 100 m depth for the north-western and south-eastern explosions, respectively called explosions I and II. Fig. 6 shows the ground velocity computed with a Ricker source pulse central frequency of 3.5 Hz, at stations distributed from 31 km to the north-west to 31 km to the south-east of both explosions. The time duration is 13 s.

The first arrival is a P wave (P_A^{nw} and P_A^{se}) that propagates alone in both azimuths for explosion I, while it consists of two pulses (P_{A1}^{nw} and P_{A2}^{nw}) delayed by 0.8 s in the north-west and one pulse in the south-east (P_A^{se}) for explosion II. The inverted polarity and amplitude variation of P_{A2}^{nw} compared to P_{A1}^{nw} may indicate that the second pulse has been generated by reflection of the direct P wavefield inside the mountain.

The surface waves show a more complex shape and amplitude behaviour for explosion I than for explosion II.

(1) The relative amplitude in the north-west azimuth is 25 per cent and 40 per cent lower than the one obtained in the south-east for explosions I and II respectively.

(2) Waveforms of R_A^{nw} and $R_{C(A)}^{nw}$ phases have a higher frequency content for explosion I than has the R_A^{nw} phase for explosion II.

(3) In the case of explosion I, the main surface Rayleigh wave train, R_A^{nw}, is followed by a coda, $R_{C(A)}^{nw}$, which may consist of a back-diffracted surface wave inside the south-eastern side of the massif. The symmetric observation of such a coda cannot be made for explosion II, i.e. this observation implies that the hillside steepness strongly shapes the back-diffracted field.

A detailed comparison of the ground velocities at 21 km is displayed in Fig. 7 for both explosions. Besides the

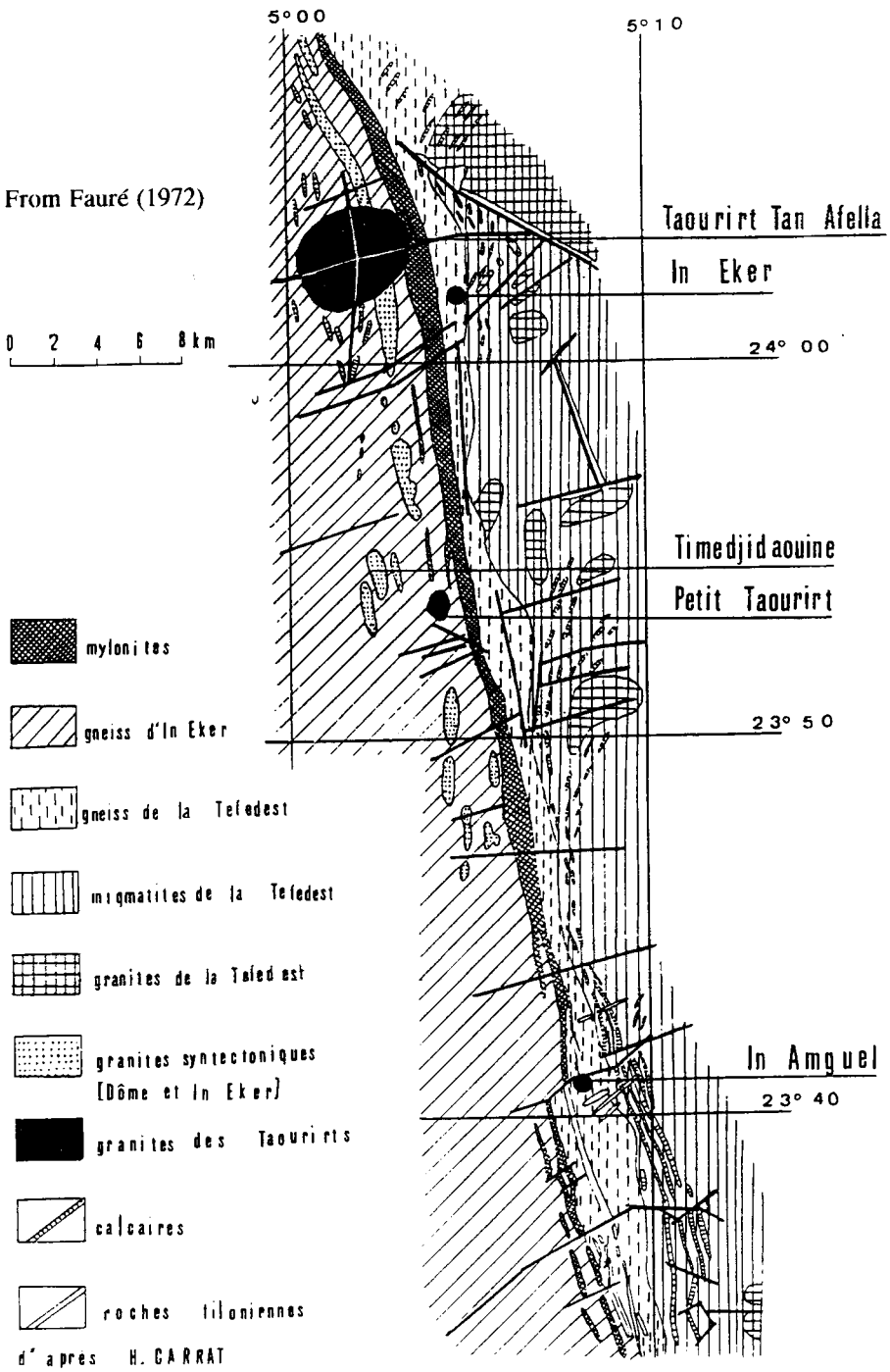

Figure 2. This map, from Fauré (1972), illustrates the geological formation located around the Taourirt tan Afella test site.

Table 1. Location of the ground velocity recorders.

Code	Lat N	Lon E
BRI	*24 02 07.7*	*05 01 17.8*
BRIII	*24 02 00.8*	*04 55 01.9*
INA	*23 47 30.0*	*05 07 30.0*

waveform differences observed between north and south, the relative amplitude given in Fig. 7 shows that the surface ellipticity (called ε, and defined here by the ratio H_{max}/Z_{max}) of the Rayleigh wave remains constant, whatever the azimuth is, for a given explosion location. On the other hand, ellipticity varies when source location changes, i.e. $\varepsilon_I \approx 0.60$ and $\varepsilon_{II} \approx 0.80$ while $\varepsilon \approx 0.6812$ (Ben-Menahem & Singh 1981) should be obtained without mountain topography and a Poisson ratio of 0.25 as used in this paper. Thus, the phase velocity of the main Rayleigh wave train is modified by source site condition.

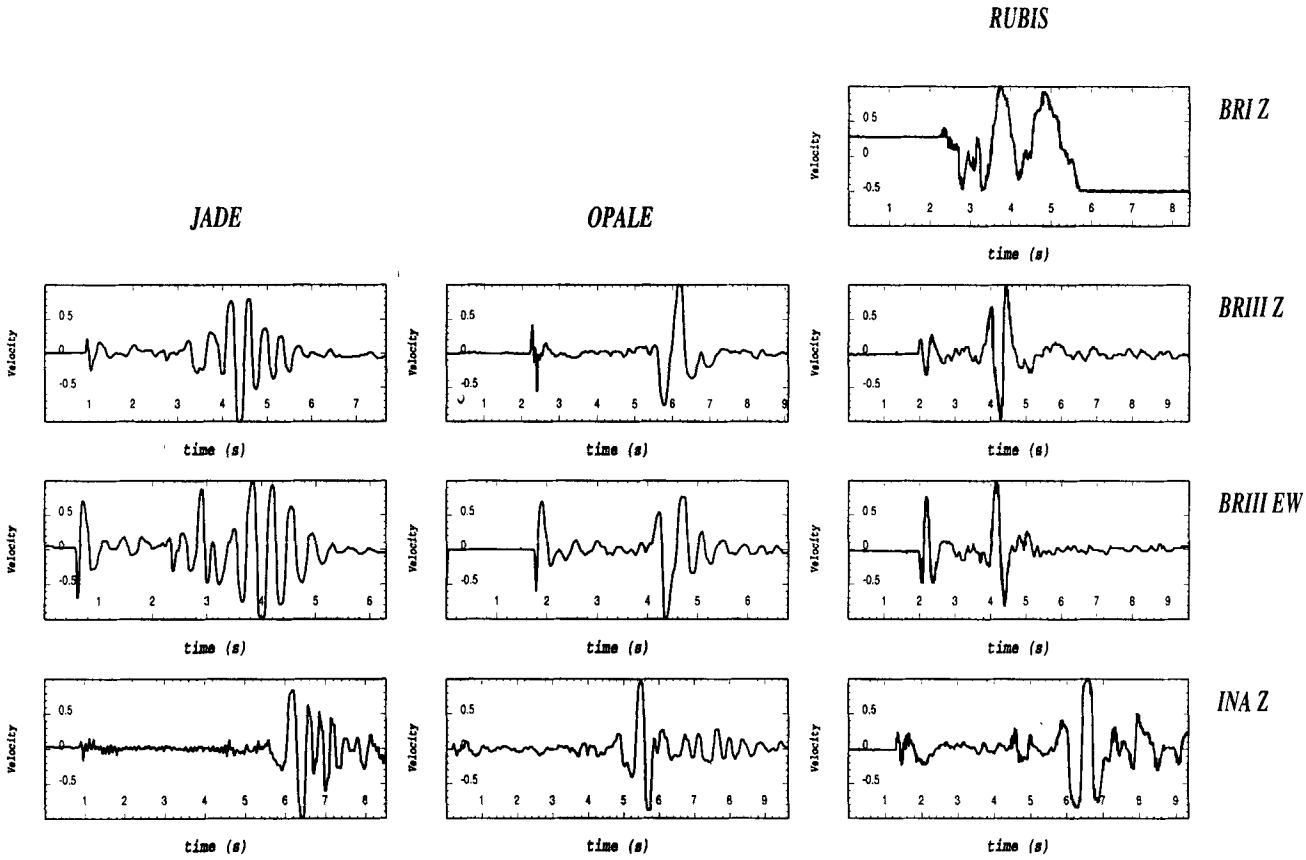

Figure 3. Ground velocity recorded for Jade, Opale and Rubis at locations BRI for Rubis, and BRIII and INA for Jade, Opale and Rubis. Locations of receivers are shown in Table 1.

Figure 8 displays the realistic geographical configurations that correspond to explosions Jade, Opale and Rubis. The sections and relative explosion locations obtained for Jade and Opale are so similar at the wavelengths studied, i.e. $\lambda_\beta \approx 1$ km (see right side of Fig. 7), that they will now be considered as one detonation point. This means that the Rayleigh waveform differences observed at BRIII (Fig. 3) cannot now be associated with the topographical effects studied but should be related to the explosion source itself. Besides the N–S section for Rubis and the two W–E sections, the N–S section related to Jade/Opale does not respect any cylindric aspect, i.e. in this case, results obtained by the corresponding 2-D simulation will be solely descriptive and should be cautiously related to real data such as those mentioned hereafter, at INA for instance.

Taking into account the previous remark, Figs 9 and 10 display the ground velocities calculated in N–S and E–W azimuths for explosions Jade/Opale and Rubis. The source pulse is a Ricker function centred at 3.5 Hz. The time-window duration is 13 s. Explosion Jade/Opale is buried at 370 m vertical and 310 m normal depths, the explosion Rubis is buried at 550 m vertical and 450 m normal depths. Explosion Jade/Opale is located inside the mountain i.e. approximately 100 m above the 1000 m mean elevation of the surrounding tableland, while explosion Rubis is buried at a level approximately 100 m under this 1000 m elevated plateau.

The phases noted P_B^{north} and R_B^{north} (Fig. 9) show similar waveforms for both explosion sites Jade/Opale and Rubis. Though R_B^{north} has a longer duration of large-amplitude oscillations for Rubis, i.e. approximately one cycle more, compared to Jade/Opale, the relative amplitude of the surface wave train R_B^{north} of Jade/Opale is 1.5 times the relative amplitude for Rubis at epicentral distances greater than 15 km. The relative amplitudes obtained in the N–S azimuth are very different between both sites. The relative amplitude for Jade/Opale is 2.5 times the one for Rubis; this result reproduces well the observation of P and Rayleigh wave-amplitude ratio at station INA (Fig. 3). Rubis shows a longer Rayleigh wave train R_A^{south}, followed by a coda $R_{C(A)}^{\text{south}}$, than R_A^{south} for explosion Jade/Opale.

The W–E section ground velocities are compared in Fig. 10 for both sites. The topographic heterogeneity dimensions of the two configurations are 5 km long × 1 km height for Jade/Opale and approximately 3 km long × 0.5 km height for Rubis. This implies that coupling wavelengths for Rubis should be reduced by half compared to Jade/Opale. Such an effect is clear in the eastern azimuth with R_B^{east} frequency behaviour between both sites, while it does not appear in the western azimuth. Two consecutive P waves, P_{A1}^{west} large and P_{A2}^{west} low amplitudes, delayed by 0.8 s, are generated at the explosion site corresponding to Jade/Opale. This minor second phase may be a diffracted P surface wave, its time delay and small amplitude being induced by the propagation along the mountain topography. The Rayleigh wave train, R_A^{west} generated at the Jade/Opale site has a longer time duration, 1.7 s, and a smaller relative amplitude than that observed for Rubis. It also shows a low-amplitude Rayleigh

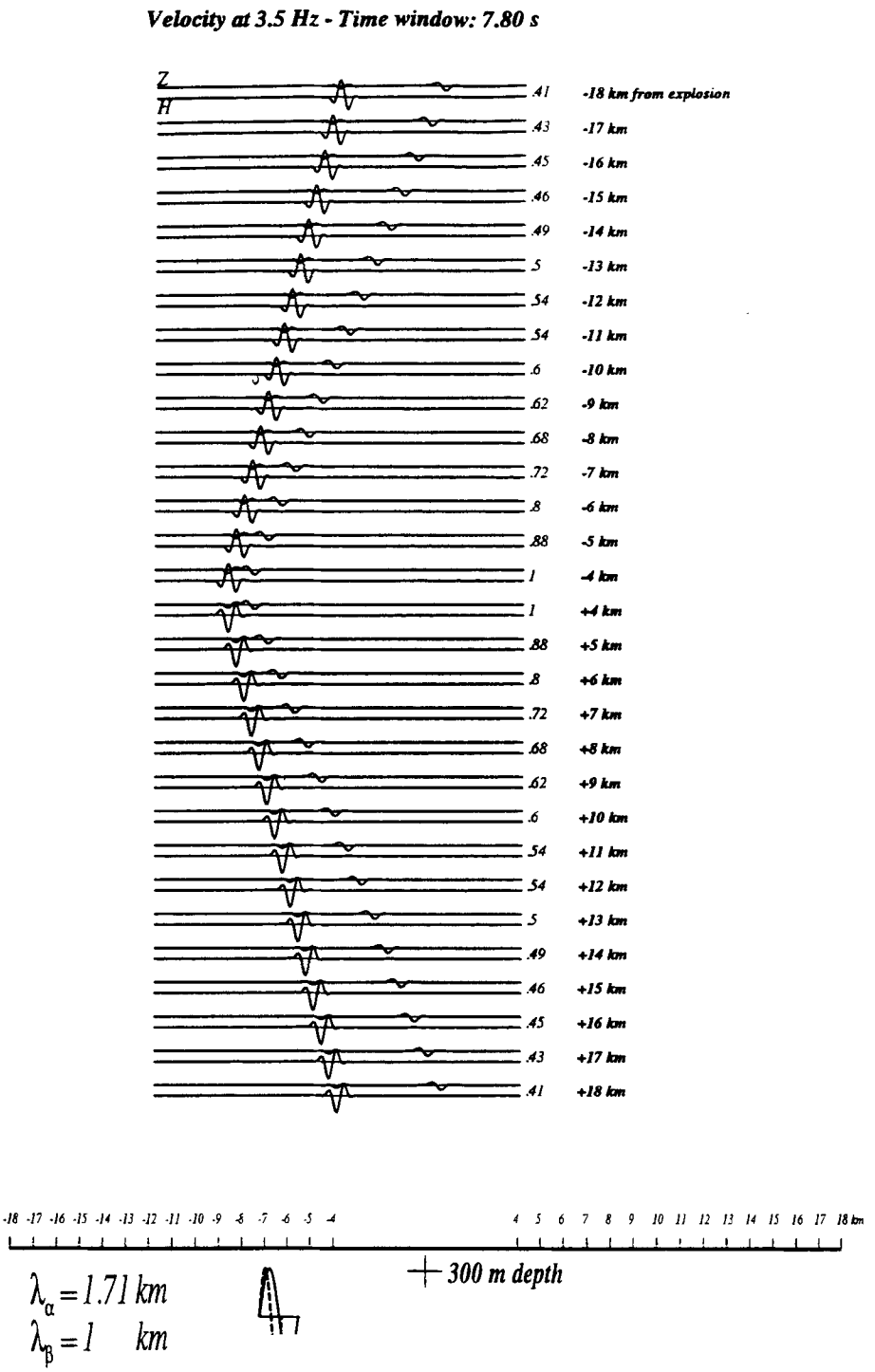

Figure 4. Horizontal (H) and vertical (Z) components of the ground velocity computed for an exposion buried at 300 m depth under a flat surface in a homogeneous space. The source is a Ricker pulse centred at 3.5 Hz. The time window is 7.8 s. Receivers are identified by their epicentral distances (from −18 km to +18 km).

wave train that arrives before the main surface wave train, and this precursor does not appear for the Rubis site.

A general observation of stacks presented in Figs 9 and 10 is that seismograms obtained in the N–S azimuth show more complex time duration, waveform and frequency content behaviours than those calculated for the W–E section. This observation may be related to a more complex N–S topography shape (see Fig. 8), therefore inducing a more complex wave diffraction scheme by topography than the one for the W–E section.

A detailed comparison between ground-velocity components calculated at 21 km epicentral distance from each side, i.e. azimuths, for both Jade/Opale and Rubis sites is displayed in Fig. 11. The different phases discussed previously are labelled above each component. A new time, surface ellipticity, based on the relative amplitudes found for

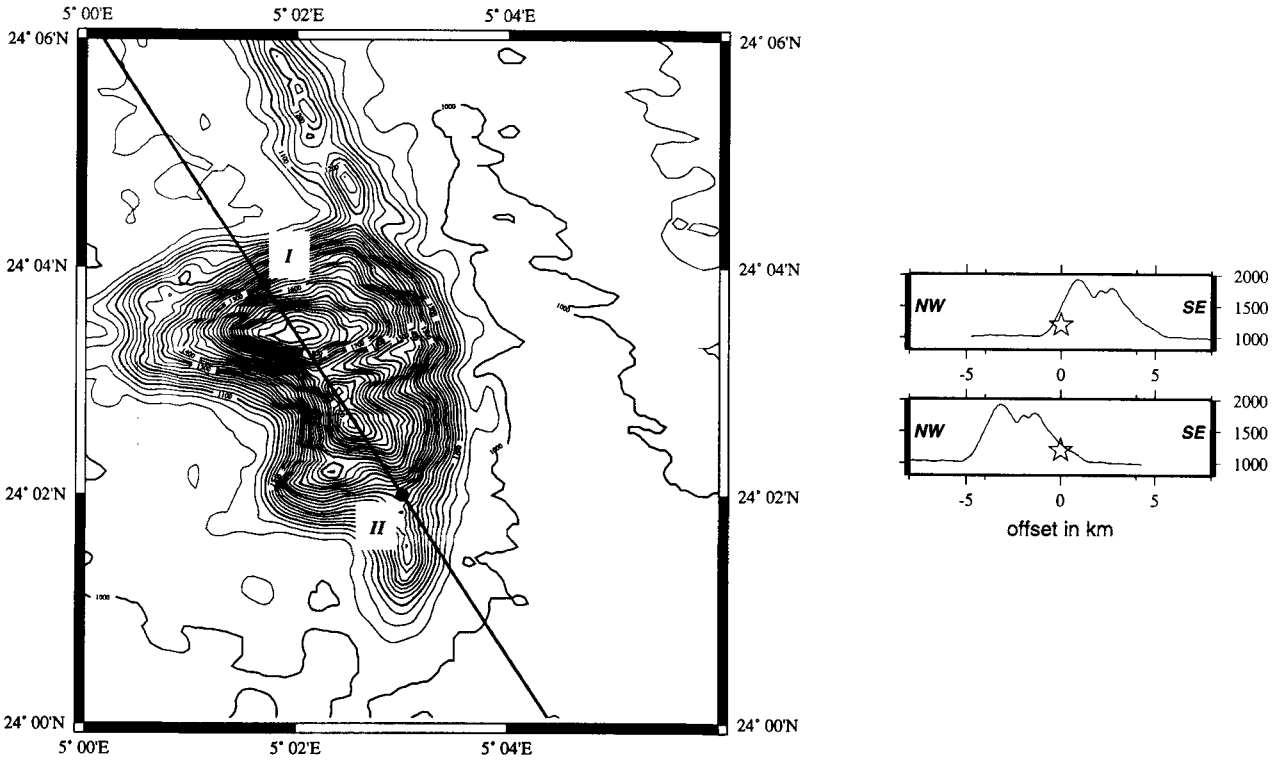

Figure 5. Geometrical configuration used to compute the seismograms presented in Figs 6 and 7. A NW–SE section crosses the tan Afella massif with two fictitious explosions called I and II in the text. Locations in 1-D section are given on the right side, with elevation in metres and offset from explosion in kilometres.

each component, remains constant whatever the azimuth is and appears to be sensitive to both topographic heterogeneity shape and explosion location. $\varepsilon \approx 0.68$ for explosion Jade/Opale in the N–S azimuth, $\varepsilon \approx 0.62$ in the W–E azimuth while $\varepsilon \approx 0.72$ for explosion Rubis in the N–S azimuth and $\varepsilon \approx 0.64$ in the W–E azimuth.

The different components stacked in Fig. 11 align both *P* arrivals and the main Rayleigh wave trains, i.e. $R_{A \text{ or } B}^{\text{north or south}}$. Precursors are depicted before the main Rayleigh wave train for explosion Jade/Opale in the west and for explosion Rubis in the north. These precursors are generated with a similar and symmetric diffraction scheme (see the W–E section for Jade/Opale and the N–S section for Rubis in Fig. 8). These precursors are generated by the direct *P* wavefield diffracted into Rayleigh wave on the opposite side of the mountain while the main Rayleigh wave train is generated by the direct *P* wavefield diffracted into Rayleigh wave on the nearby topography. Except for explosion Rubis in the N–S section, the main frequency content varies from one side to the other for each section and explosion. It appears that the more the topography steepens, the lower the frequency of the main Rayleigh wave train becomes. This phenomenon appears simultaneously on both components. Such behaviour is not seen for Rubis at the N–S section, which it may be explained by identical steepness on both sides of the mountain.

Table 2. French explosions and their characteristics.

Explosion	Date	Time UT	Lat N	Lon E	m_b
Agate	1961/11/07	11h 29m 59.931s	24° 3′ 25.5″	5° 3′ 7.6″	
Beryl	1962/05/01	10h 00m 00.458s	24° 3′ 46.8″	5° 2′ 30.8″	
Emeraude	1963/03/18	10h 02m 00.351s	24° 2′ 28.9″	5° 3′ 7.9″	
Amethyste	1963/03/30	09h 59m 00.328s	24° 2′ 36.0″	5° 3′ 25.2″	
Rubis	1963/10/20	13h 00m 00.011s	24° 2′ 7.8″	5° 2′ 19.0″	5.6 (*USGS*)
Opale	1964/02/14	11h 00m 00.347s	24° 3′ 13.1″	5° 3′ 8.6″	
Topaze	1964/06/15	13h 40m 00.367s	24° 3′ 59.8″	5° 2′ 4.4″	
Turquoise	1964/11/28	10h 30m 00.035s	24° 2′ 30.7″	5° 2′ 30.1″	
Saphir	1965/02/27	11h 30m 00.039s	24° 3′ 31.4″	5° 1′ 52.3″	5.8 (*USGS*)
Jade	1965/05/30	11h 00m 00.037s	24° 3′ 18.0″	5° 3′ 3.1″	
Corindon	1965/10/01	10h 00m 00.043s	24° 3′ 53.7″	5° 2′ 2.6″	
Tourmaline	1965/12/01	10h 30m 00.088s	24° 2′ 37.4″	5° 2′ 48.9″	5.1 (*USGS*)
Grenat	1966/02/16	11h 00m 00.035s	24° 2′ 39.0″	5° 2′ 28.4″	

4 CONCLUSION

The results show the great influence of topography on the ground velocity recorded in the frequency band 1–4 Hz, at epicentral distances from 3 to 31 km for three explosions detonated inside the granitic massif of the Taourirt tan Afella. The general result is that the topography alone strongly shapes the ground velocities, their amplitudes and their frequency contents.

The main results are as follows.

(1) The back-scattered wave strongly shapes the seismograms. The surface wave appears to be generated after

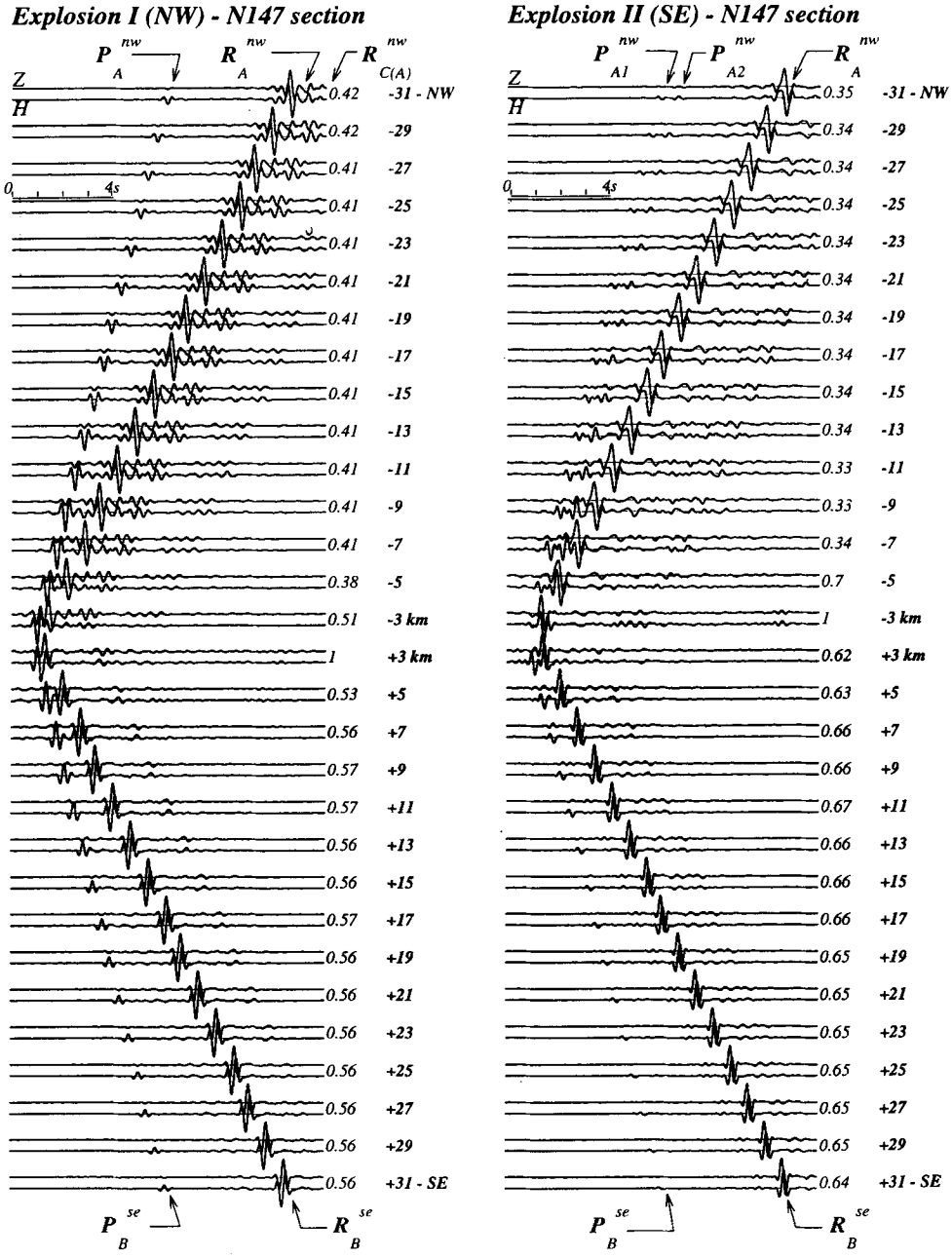

Figure 6. Comparison of ground velocity computed at epicentral distances of 3–31 km from each side of the mountain, for explosions I (left side) and II (right side). The first column in the right side of each stack gives the relative amplitude for each explosion, the second column gives the epicentral distances. See text for explanation. Time duration is 13 s and source time function is a Ricker pulse centred at 3.5 Hz.

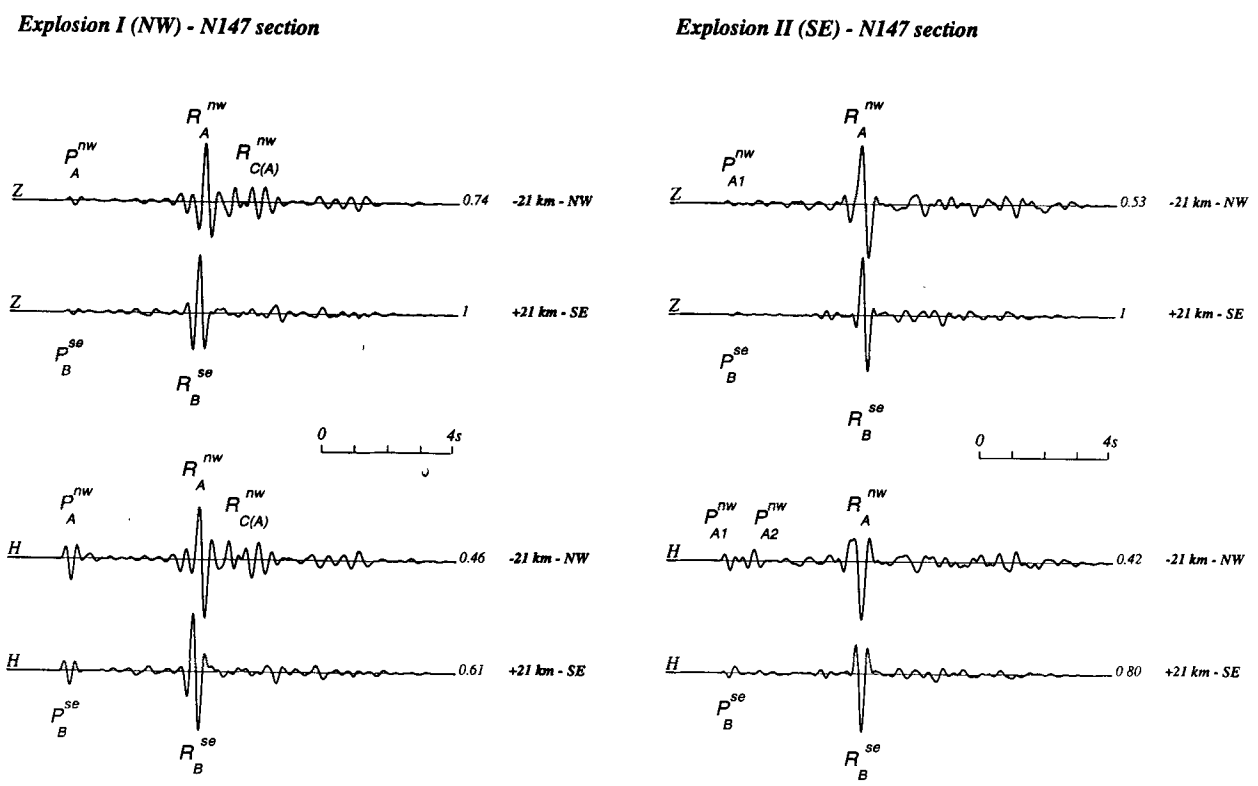

Figure 7. Comparison of the NW and SE horizontal and vertical ground-velocity components recorded for explosions I and II at 21 km epicentral distance. The names of different phases are given with their significances explained in the text. Relative amplitudes are given for each component and for each detonation point.

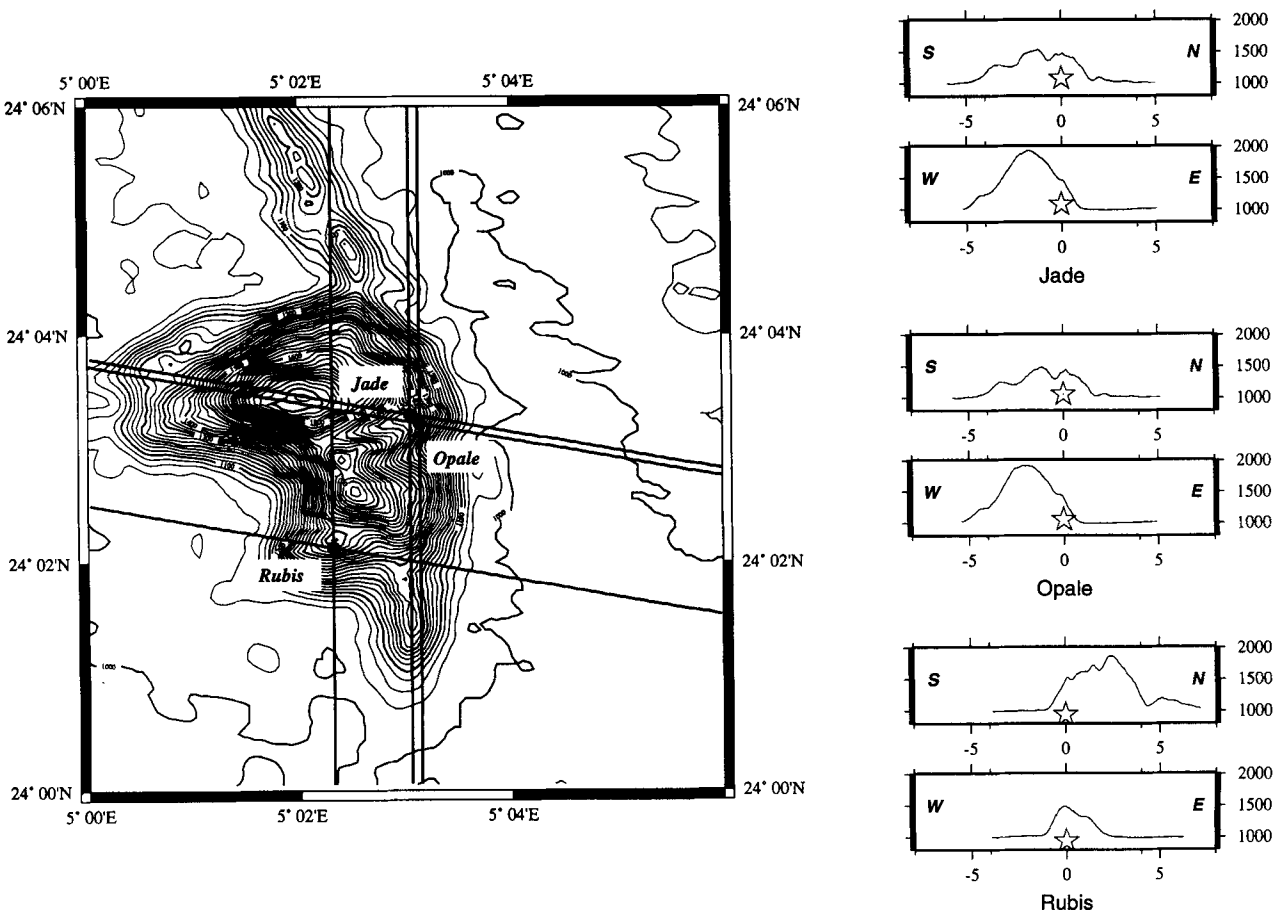

Figure 8. Realistic configuration for Jade, Opale and Rubis. Two 2-D sections (N–S and W–E) are reported on the right side for each detonation point. Elevation and offset from shot are given in metres and in kilometres, respectively.

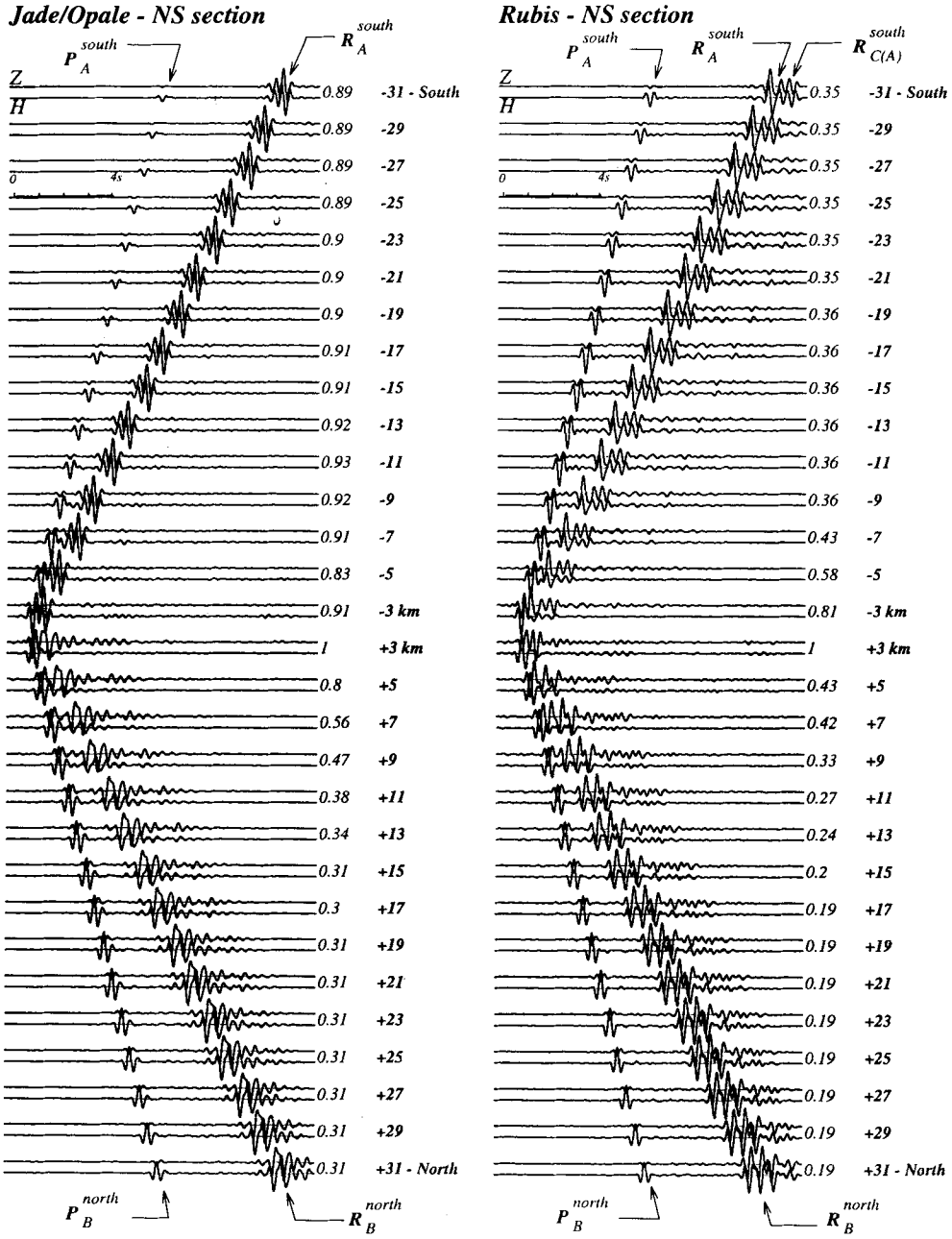

Figure 9. Stacks of ground velocities for explosions Jade/Opale and Rubis and receivers in the N–S section. The time duration is 13 s and the source function is a Ricker pulse centred at 3.5 Hz. Relative amplitude for each explosion and negative, i.e. southern azimuth, and positive, i.e. northern azimuth, offsets from explosions are reported in the right side first and second column respectively of each stack. Different phases are labelled and discussed in the text.

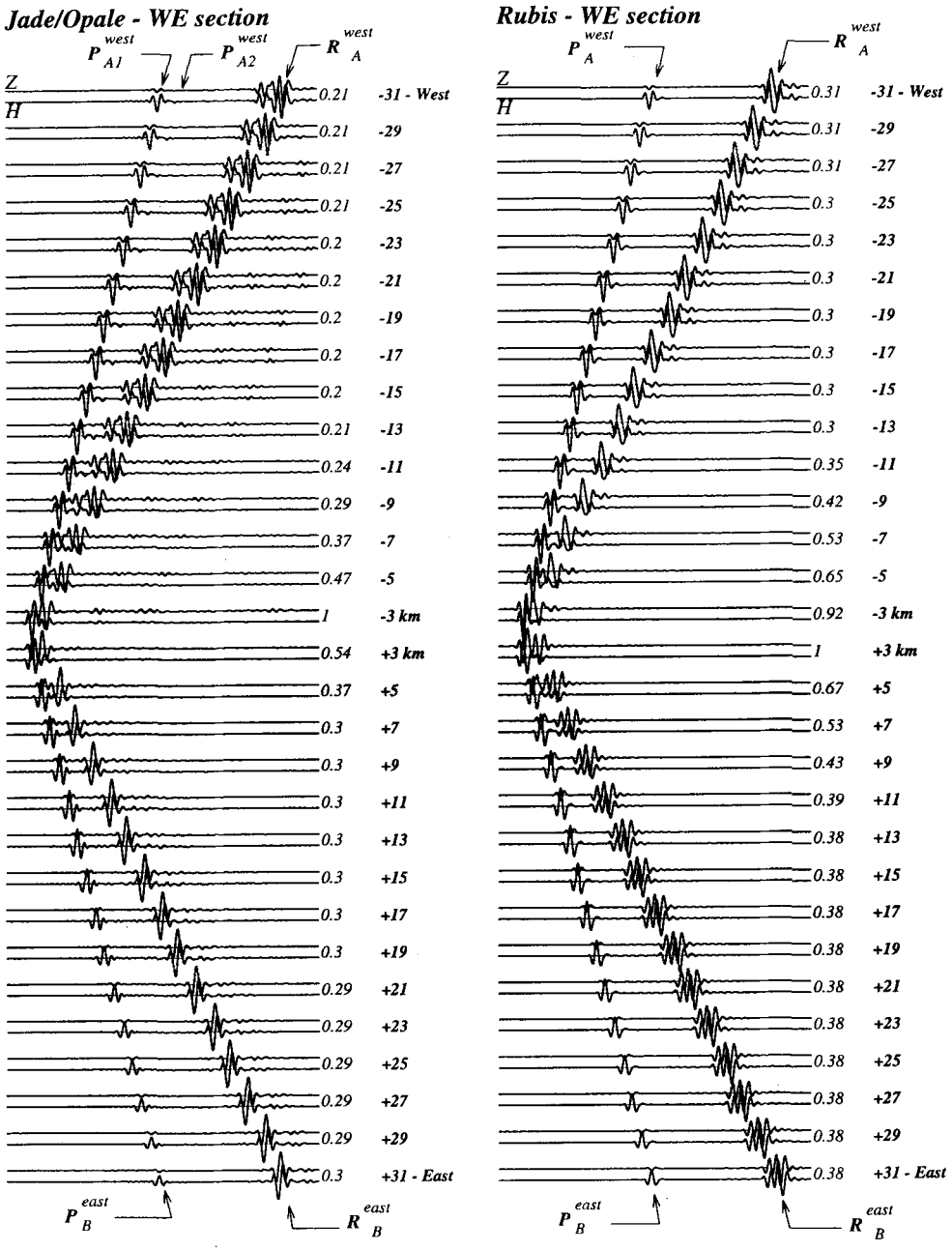

Figure 10. Same as Fig. 9 but for the W–E section displayed in Fig. 8.

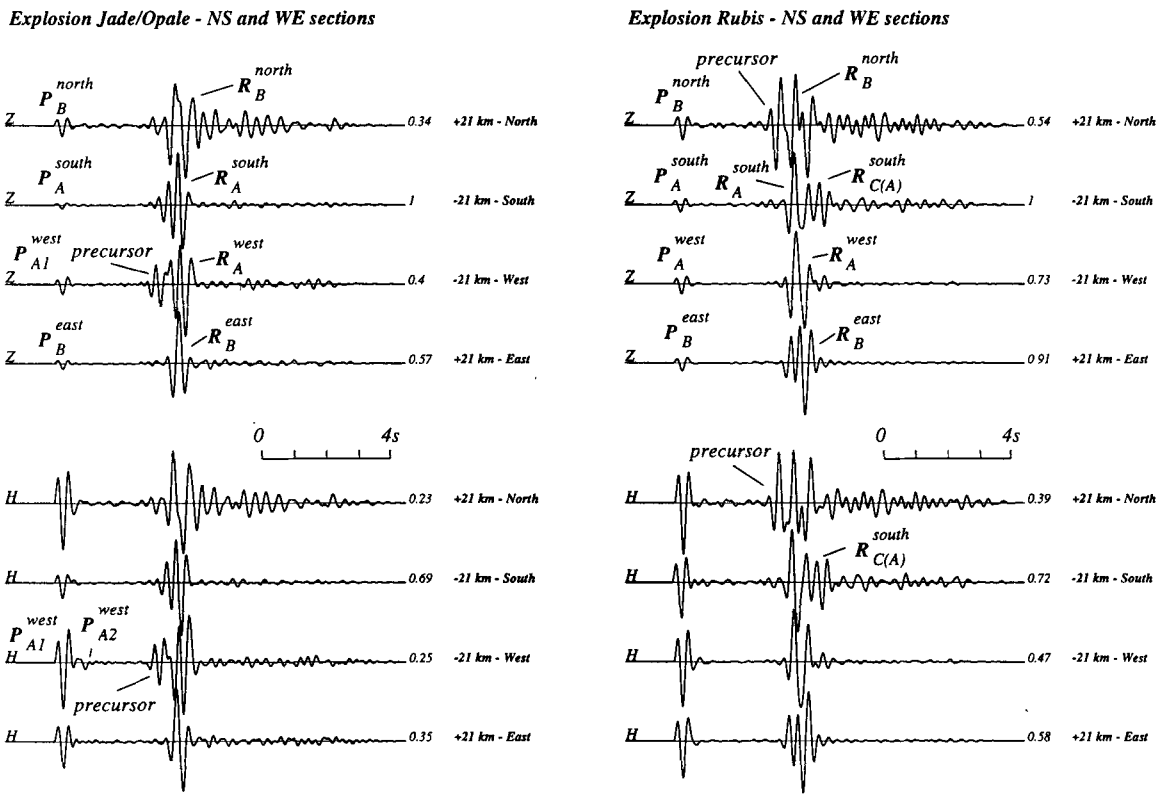

Figure 11. Comparison of the N, S, W and E horizontal and vertical ground velocity components calculated for explosions Jade/Opale and Rubis at 21 km epicentral distance. The relative amplitudes are given for each explosion and component. Source–time function and window duration are those defined in Figs 9 and 10. Phases labelled in Figs 9 and 10 are reported and discussed in the text.

diffraction of the direct field onto both the opposite and the nearby sides of the massif.

(2) The back-scattered field is made up of both a *P* surface wave and a Rayleigh wave train.

(3) We show that for a receiver located at the same epicentral distance, the amplitude of the vertical ground velocity may vary with a factor of 3, from one side of the massif to the other.

(4) We show that the duration of the surface wave train may be strongly enlarged depending on the azimuth of observation.

(5) Precursors to the main Rayleigh wave trains may exist, depending on diffraction conditions of the direct *P* wavefield.

(6) The steepness of the topography determines the frequency content.

ACKNOWLEDGMENTS

This work was supported by the Advanced Research Projects Agency and was monitored by the Air Force Office of Scientific Research under Grant 90-0356.

REFERENCES

Ben-Menahem, A. & Singh, S.J., 1981. Seismic waves and sources, Springer-Verlag, New York.

Bouchon, M. & Aki, K., 1977. Discrete wavenumber representation of seismic source wave fields, *Bull. seism. Soc. Am.*, **67,** 259–277.

Boullier, A.-M. & Bertrand, J.-M., 1981. Tectonique tangentielle profonde et couloirs mylonitiques dans le Hoggar central polycyclique (Algérie), *Bull. Soc. géol. France,* **XXXIII,** 17–22.

Duclaux, F. & Michaud, L., 1970. Conditions expérimentales des tirs nucléaires souterrains français, 1961–1966, *C. R. Acad. Sci. Paris,* **270,** 189–192.

Fauré, J., 1972. Recherche sur les effets géologiques d'explosions nucléaires souteraines dans un massif de granite Saharien, *Report CEA-R-4257.*

Gaffet, S. & Bouchon, M., 1989. Effects of two-dimensional topographies using the discrete wavenumber—boundary integral equation method in *P–SV* cases, *J. acoust. Soc. Am.,* **85,** 2277–2283.

McLaughlin, K.L. & Jih, R.-S., 1988. Scattering from near source topography: teleseismic observations and numerical simulations, *Bull. seism. Soc. Am.*, **78,** 1399–1414.

Munier, G., 1982. Construction d'un modèle de croûte sous le Hoggar Central, *Report CEA/LDG 53-82.*

Rocard, Y., 1964. Formation du signal séismique lors d-une explosion souterraine, *C. R. Acad. Sci. Paris,* **258,** 2373–2375.

Wessel, P. & Smith, W.H.F., 1991. Free software helps map and display data, *EOS Trans. Am. geophys. Un.,* **72,** 441.